Dynamic Event-Triggered Adaptive Control of a Flexible Manipulator With Output Quantization

Zhijia Zhao, *Senior Member, IEEE,* Rourou Xu, Zhifeng Tan, Shouyan Chen, Junfeng Zhang, Zhijie Liu, *Member, IEEE*, Keum-Shik Hong, *Fellow, IEEE*

***Abstract*—This study presents a novel adaptive dynamic event-triggered quantized control strategy for a flexible manipulator system. Initially, output signal is quantized using a uniform quantizer that account for the communication burden and bandwidth constraints. Subsequently, a dynamic event-triggered mechanism is devised to further decrease the frequency of control input communication. The proposed control strategy enables the angular tracking and tip vibration of the flexible manipulator system to exponentially converge to a small compact set under limited communication. Finally, the effectiveness of the design scheme is demonstrated through simulations and experimental validations.**

***Index Terms*—Flexible manipulator, adaptive control, dynamic event-triggered mechanism, output quantization.**

I. Introduction

In recent years, there has been an increasing demand for continuous advancements in robotic technology, especially manipulators [1]–[3]. Flexible single-link manipulator (FSLM) possess the benefits of reduced energy usage, high flexibility, and low weight, which has broader application prospects than rigid manipulators. However, the characteristics of the FSLMs expose them to structural vibrations that can lead to deformations, which decreases their precision and lifespan [4]. Hence, eliminating vibrations in the working environment of the FSLMs is necessary to maximize their performance.

As distributed-parameter systems, FSLMs should be modeled using partial differential equations (PDEs) [5]. To facilitate analysis, a number of researchers have developed an FSLM control strategy using the modal method [6], [7], but this may cause a spillover effect. Because only a few sensors and actuators are required and there is no need to simplify the model, boundary control has been recently regarded as a more practical control method for the FSLMs [8], [9]. In [10], a boundary control method for a robotic manipulator system was proposed, and novel observers and auxiliary systems were introduced to address unknown disturbances and input constraints. In addition, the authors in [11] examined an adaptive robust boundary control scheme that handled the input dead zone and estimated the upper limit of compound disturbances for a flexible Timoshenko manipulator. Furthermore, in [12], an adaptive neural network fault-tolerant control strategy was employed for an FSLM with model uncertainties and an infinite set of time-varying actuator faults. Additionally, a cooperative fault-tolerant control boundary method was established for a mobile dual FSLM to handle the constraint of the system outputs and actuator failures in [13]. Despite these beneficial results, the methods in these studies were not applied to the FSLM system with quantization.

In network control systems [14], it is common to quantize signals to reduce the communication burden. However, this action inevitably introduces certain nonlinear characteristics that will affect system performance if neglected. In the last few years, researchers have investigated this problem, and a number of quantized control schemes have been developed for nonlinear systems of the ordinary differential equation (ODE) [15]–[17]. Advances have also been made in quantization control for the FSLM systems as a result of research on ODE systems. [18]–[20]. In [18], two different quantization controllers were proposed for a FSLM system with input-signal quantization. For a FSLM system with communication constraints [20], an adaptive boundary control strategy was presented to compensate for the quantization error. The aforementioned studies investigated input quantization, but recently there has been an increasing interest in output quantization. For example, in [21], a control methodology based on adaptive backstepping was introduced for a specific category of rigid body systems characterized by multiple inputs and multiple outputs, considering the presence of both input and output quantization. Additionally, in [22], an adaptive output feedback control scheme was presented for nonlinear systems with mismatched uncertainties under input and output quantization, and a dynamic filtering technique was employed to avoid differentiating the virtual control signals. The existing output quantization schemes were primarily relevant for ODE systems, and studies on output quantization for the FSLM systems have been scarce; this is one of the motivations for this study.

This work was supported in part by the National Natural Science Foundation of China under Grant 62273112, Grant 62473039, Grant 62433011, Grant 62573144, and Grant 62522305, in part by the Guangdong Basic and Applied Basic Research Foundation under Grant 2024B1515120013, Grant 2023B1515120018, and Grant 2023B1515120019, in part by the Science and Technology Planning Project of Guangzhou, China under Grant 2025A03J3135 and Grant 2025A04J5629in part by the Joint Fund of Ministry of Education for Equipment Pre-Research under Grant 8091B03032303, and in part by Beijing Nova Program under Grant 20240484561. *(Corresponding authors: Zhijia Zhao.)*

Zhijia Zhao, Rourou Xu, Zhifeng Tan and Shouyan Chen are with the School of Mechanical and Electrical Engineering, Guangzhou University, Guangzhou 510006, China. (e-mail: zhjzhaoscut@163.com; xurourou49@163.com; 2112107119@e.gzhu.edu.cn;maxcsy@gzhu.edu.cn).

Junfeng Zhang is with the School of Information and Communication Engineering, Hainan University, Haikou, 570228, China (e-mail: jfzhang@hainanu.edu.cn).

Zhijie Liu is with the School of Intelligence Science and Technology, University of Science and Technology Beijing (USTB), Beijing 100083, China (e-mail: liuzhijie@ustb.edu.cn).

Keum-Shik Hong is with the School of Mechanical Engineering, Pusan NationalUniversity, Busan 46241, Republic of Korea (e-mail: kshong@pusan.ac.kr).

Furthermore, in a general control system, the output of the controller is continuously transmitted, and frequent nonessential transmissions waste the system's limited resources. Event-triggered control (ETC) has garnered considerable attention in recent years, as it enables systems to update control input signals only when specific conditions are met, thereby reducing communication frequency [23]–[25]. In [26], a backstepping adaptive event-triggered feedback control strategy was developed for a class of uncertain nonlinear systems, effectively addressing the challenges posed by discontinuous output signals and reduces unnecessary control input updates. Furthermore, an adaptive controller and a triggering event based on the switching threshold strategy were designed simultaneously for a class of uncertain nonlinear systems, avoiding the input-to-state stability assumption [27]. Recently, researchers have achieved progress in the ETC of FSLMs. In [28] and [29], event-triggered boundary control schemes for FSLMs under communication constraints were proposed. As far as we are aware, despite significant progress being achieved in the ETC of FSLMs, the aforementioned event-triggered mechanisms were based on the relative threshold strategy. The relative threshold event-triggered mechanism (ETM) utilizes static rules, where the event-triggering conditions remain constant over time. In contrast, the dynamic event-triggered mechanism (DETM) incorporates internal dynamic variables, making the triggering conditions more adaptable [1], [30]. This adaptability enables the system to determine control input updates with greater flexibility, effectively minimising unnecessary communication and computational overhead. In [31], to address the distributed formation control problem of networked multi-agent systems under limited communication resources, a DETM was proposed, in which the threshold parameters of the triggering conditions can be modified dynamically. Currently, there are no studies in the literature on the DETM control for FSLMs and considering the output quantization of the system on this basis is more challenging.

Based on the afore-described analysis, the objective of this study is to investigate the dynamic ETC problem for an FSLM system with output quantization. The primary contributions of this research are outlined as follows:

1) In contrast to the research [20], [32] in which input quantization is considered, the discrete phenomena of the output quantization for the flexible system pose greater challenges to the controller development and stability analysis. Hence, in this paper, we consider the impact of output quantization on the FSLM system, and an inequality descibing the measured signals and the quantizer parameters is utilized to transfrom the quantization error.
2) Previous studies on event-triggered strategies for the FSLMs were based on the relative threshold [28], [33]. We propose a DETM that includes an adaptive dynamic variable, which adjusts according to the measurement error, to alter the frequency of communication more flexibly without gravely degrading the system performance.
3) The practicality and efficacy of the proposed scheme are confirmed through simulations performed in MATLAB and experiments conducted on the Quanser platform.

Remark 1: Throughout this paper, the sets of all positive integers and real numbers are denoted by $\mathbb{Z}_+$ and $\mathbb{R}$, respectively. For the sake of simplifying the expression, the following symbols are introduced: $(*)' = \partial(*)/\partial s$, $(*)'' = \partial^2(*)/\partial s^2$, $(*)''' = \partial^3(*)/\partial s^3$, $(*)'''' = \partial^4(*)/\partial s^4$, $(\dot{*}) = \partial(*)/\partial t$, $(\ddot{*}) = \partial^2(*)/\partial t^2$, $(*) = (*)(s,t)$, $(*)_0 = (*)(0,t)$, and $(*)_l = (*)(l,t)$.

II. Problem Statement

A. System description

A simplified representation of the geometry of the FSLM system is shown in Fig. 1. In the figure, $\mathcal{X}O\mathcal{Y}$ represents the global fixed coordinate system; the local rotating inertial coordinate system is denoted by x_1oy_1; the independent time and space variables are represented by t and s, respectively; l is the length of the manipulator; $u_r(t)$ represents the torque input; $\omega(s,t)$ represents the vibrational displacement in the rotating coordinate system; $\theta(t)$ is the angular displacement; and $\varpi(s,t) = s\theta(t) + \omega(s,t)$ is defined as the position of variable s in the coordinate axis $\mathcal{X}O\mathcal{Y}$.

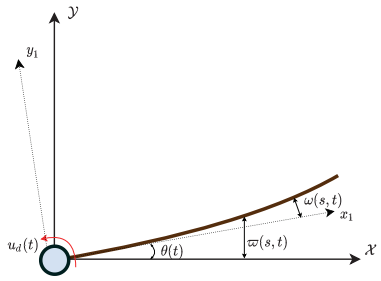

Fig. 1. Flexible manipulator system.

The PDEs describing the FSLM system are given as [34]:

$$\rho\ddot{\varpi}(s,t) = -\flat\dot{\varpi}(s,t) - EI\omega''''(s,t) + T\omega''(s,t)$$
$$\forall(s,t) \in (0,l) \times [0,+\infty) \tag{1}$$

The boundary conditions are presented as follows:

$$I\ddot{\theta}(t) = EI\omega''(0,t) + T\omega(l,t) + u_r(t) \quad t \in [0,+\infty) \tag{2}$$
$$EI\omega'''(l,t) = T\omega'(l,t) \tag{3}$$
$$\omega(0,t) = \omega'(0,t) = \omega''(l,t) = 0 \tag{4}$$

where, T, ρ, $\flat$, I, and EI represent the tension, constant mass per unit length, coefficient of viscous damping, hub inertia, and bending stiffness, respectively.

B. Quantizer

The quantizers considered in this study have the following properties:

$$|k^Q - k| \leq k_{\min} \tag{5}$$

where $k_{\min} > 0$ are quantization parameters. k^Q and k are quantized and ideal signals, respectively.

This article has been accepted for publication in IEEE Transactions on Consumer Electronics. This is the author's version which has not been fully edited and content may change prior to final publication. Citation information: DOI 10.1109/TCE.2025.3610905

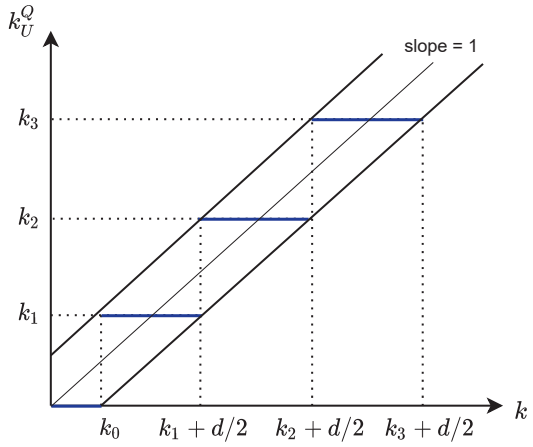

Fig. 2. The map of uniform quantizer k_U^Q.

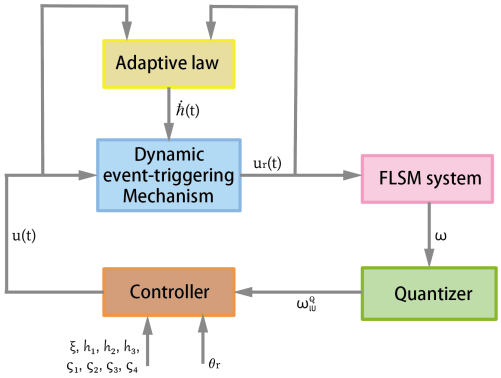

Fig. 3. The control process of the FSLM system.

Uniform Quantizer: The model of uniform quantizer is given as ([21]):

$$k_U^Q = \begin{cases} k_i sgn(k), & k_i - \frac{d}{2} < |k| \le k_i + \frac{d}{2} \\ 0, & |k| \le k_0 \end{cases} \tag{6}$$

where $k_0 > 0$, $k_1 = k_0 + \frac{d}{2}$, and $k_{i+1} = k_i + d$ with i=2,...; variable $d > 0$ denotes the length of the quantization interval; and $k_U^Q \in \{0, \pm k_i\}$. A map of the uniform quantizer is shown in Fig. 2. Clearly, while $|k_U^Q - k| \le k_{\min} = \max\{k_0, d\}$, property (5) is satisfied.

III. Control Design

In this section, a dynamic ETM is constructed to decrease the frequency of communication of the control input. Specifically, a dynamic Event-Triggered Output Quantized Controller (DETOQC) is developed, which integrates the dynamic ETM with output quantization techniques to track the target angle θ_r and suppress the elastic deflection $\omega(s,t)$ of the FSLM system under output quantization. Subsequently, the stability of the closed-loop system is analyzed, and it is proved that the Zeno behavior is avoided. The control flow of the FSLM system is illustrated in Fig. 3.

Remark 2: Zeno behavior refers to the occurrence of an infinite number of event triggers over a finite time interval. This phenomenon is frequently observed in ETC systems, where it may lead to excessive system responses, resulting in inefficient resource utilisation and potential stability concerns. Therefore, addressing Zeno behaviour is a crucial consideration in the design of controllers that incorporate ETMs.

A. Dynamic Event-Triggered Strategy

A dynamic parameter mechanism is presented to design the ETC method which is defined as

$$u_r(t) = u(t_j), \quad \forall t \in [t_j, t_{j+1}) \tag{7}$$

where $u(t_j)$ is a continuous input control scheme to be designed later; $u_r(t)$ is the actual control signal under the dynamic ETM. The t_j and t_{j+1}, $j \in Z^+$ represent the input update time and the next update time, respectively. The dynamic ETM is defined as

$$t_{j+1} = \inf\{t > t_j | \hbar(t) + (\delta|u(t)| - |e(t)|) \le 0\} \tag{8}$$

where $e(t) = u_r(t) - u(t)$ denotes the control signal error, and $0 < \delta < 1$ is a design parameter. Whenever (8) is activated, the time is recorded as t_{j+1}, and the control value $u_r(t_{j+1})$ is applied to the system. During the time $t \in [t_j, t_{j+1})$, the control signal $u(t_j)$ remains constant, i.e., the updating law of the dynamic variable is given as

$$\dot{\hbar}(t) = -\eta\hbar + |\gamma|(\delta|u(t)| - |e(t)|) \tag{9}$$

$$\hbar(0) = \hbar_0 \ge 0 \tag{10}$$

where η is a positive constant, and $\gamma \in \mathscr{R}$ is a design function composed of system state variables that will be provided hereinafter. η represents the decay rate, typically selected to be small. γ indicates the tightness of the dynamic event-triggering; a larger γ implies more relaxed conditions, allowing for relatively larger signal errors. The mechanism (8) guarantees that, for all times,

$$\hbar(t) + (\delta|u(t)| - |e(t)|) \ge 0 \tag{11}$$

Combining (8), (9), and (11), we infer that $\dot{\hbar}(t) + \psi\hbar(t) \ge -|\gamma|\hbar(t)$ with $\hbar_0 \ge 0$. Furthemore, $\hbar(t) \ge \hbar_0 e^{-\int_0^t (\eta + |\gamma|)dt}$, $\forall t \in [0, +\infty)$. This implies that $\hbar(t)$ is defined positively.

B. Control Algorithm Design

When the output ω is quantized, based on the quantizer property (5) we have

$$|\omega_{lU}^Q - \omega_l| \le \omega_{l\min} \tag{12}$$

By derivation and transformation, we can acquire

$$\omega - \omega_{l\min} \le \omega_{lU}^Q \le \omega + \omega_{l\min} \tag{13}$$

Futher,

$$\omega_{lU}^Q \le \omega_l + \mu\omega_{l\min} \tag{14}$$

where, $\mu \in [-1, 1]$. Hence, the DETOQC law is designed as

$$u(t) = \frac{-1}{1-\delta} \frac{\gamma u_d(t)^2}{\sqrt{\gamma^2 u_d(t)^2 + \upsilon^2}} \tag{15}$$

$$u_d(t) = h_1\gamma + (h_2+T)\omega_{lU}^{Q} + \xi I\dot{\theta} + h_3(\theta-\theta_r) + \bar{\omega}\tanh(\frac{\gamma\bar{\omega}}{J}) \tag{16}$$

where δ h_1, h_2, h_3, $\bar{\omega}$ and J are positive design parameters; $\gamma = \dot{\theta} + \xi(\theta - \theta_r)$. The dynamic event-triggering mechanism (8), DETOQC, and adaptive updating laws are designed for an FSLM system with quantizers (6) via the Lyapunov direct method.

C. Stability Analysis

This section adopts the Lyapunov direct method to perform a stability analysis. Given the dissipation of energy and the states of the FSLM system, the Lyapunov function is formulated as

$$L_k(t) = L_{k1}(t) + L_{k2}(t) + L_{k3}(t) \tag{17}$$

where

$$L_{k1}(t) = \frac{1}{2}\rho\int_0^l \dot{\varpi}^2 ds + \frac{1}{2}EI\int_0^l \omega''^2 ds + \frac{1}{2}T\int_0^l \omega'^2 ds \tag{18}$$

$$L_{k2}(t) = \frac{1}{2}I\gamma^2 + \frac{1}{2}h_3[\theta(t)-\theta_r]^2 + \hbar(t) \tag{19}$$

$$L_{k3}(t) = \xi\rho\int_0^l \dot{\varpi}(s,t)\varpi_d(s,t)ds \tag{20}$$

where $\varpi_d(s,t) = \omega + s[\theta - \theta_r]$, and we can obtain $\dot{\varpi}(s,t) = \dot{\varpi}_d(s,t)$.

Lemma 1: The Lyapunnov function (17) is positive and bounded as

$$0 \le \psi_1[L_{k1}(t) + L_{k2}(t)] \le L_k(t) \le \psi_2[L_{k1}(t) + L_{k2}(t)] \tag{21}$$

where ψ_1 and ψ_2 are positive constants.

Proof: Refer to Appendix A. □

Lemma 2: The time derivative of the Lyapunov function candidate (17) has the upper-bounded

$$\dot{L}_k(t) \le -\psi L_k(t) + \varepsilon \tag{22}$$

where ψ and $\varepsilon > 0$.

Proof: Refer to Appendix B. □

Theorem 1: For the FSLM system with output quantization described by (1)-(2), under the implemented control (15), adaptive updating law (9), and bounded initial conditions, the elastic offset and tracking error can be stabilized to a small neighborhood of zero by suitably electing the configured parameters to satisfy the constraints specified in (42)-(45). The occurrence of Zeno phenomenon can be prevented by updating the control input according to the constructed event-triggering rule.

Proof: Multiplying (22) by $e^{\psi t}$ yields

$$\frac{\partial}{\partial}[L_k(t)e^{\psi t}] \le \varepsilon e^{\psi t} \tag{23}$$

By integrating (23), we obtain

$$L_k(t) \le [L_k(0) - \frac{\varepsilon}{\psi}]e^{-\psi t} + \frac{\varepsilon}{\psi} \tag{24}$$

Using (18) and Sobolev's inequality yields

$$\frac{1}{2l}\xi T\omega^2 \le \frac{\xi}{2}T\int_0^l \omega'^2 ds \le L_{k1}(t) \le \frac{1}{\psi_1}L_k(t) \tag{25}$$

Substituting (25) into (24) yields

$$|\omega(s,t)| \le \sqrt{\frac{2l}{\xi T\psi_1}[L_k(0) + \frac{\varepsilon}{\psi}]}, \forall(s,t) \in [0,l]\times[0,+\infty) \tag{26}$$

Moreover, we get

$$\lim_{t\to\infty}|\omega(s,t)| \le \sqrt{\frac{2l\varepsilon}{\xi T\psi_1\psi}}, \forall(s,t) \in [0,l] \tag{27}$$

Similarly, with (19) we derive

$$|\theta(t) - \theta_r| \le \sqrt{\frac{2l}{h_\theta\psi_1}[L_k(0) + \frac{\varepsilon}{\psi}]}, \forall(t) \in [0,+\infty) \tag{28}$$

$$\lim_{t\to\infty}|\theta(t) - \theta_r| \le \sqrt{\frac{2l\varepsilon}{h_\theta\psi_1\psi}} \tag{29}$$

□

Finally, we prove that the dynamic event-triggered strategy (8) constructed in this study can prevent the Zeno phenomenon, which can be attributed to the presence of a positive constant $t^* > 0$ that causes $t_{j+1} - t_j \ge t^*, \forall j > 0$. According to $e(t) = u_r(t) - u(t), \forall t \in [t_i, t_{i+1})$, we have

$$\frac{d}{dt}|e| = \frac{d}{dt}\sqrt{(e*e)} = \mathrm{sign}(e)\dot{e} \le |\dot{u}| \tag{30}$$

According to (15) and the property of quantification, $\dot{u}$ is a function of the quantized signals θ, $\dot{\theta}$, and ω_l, for which the changing amplitude is always bounded within the quantized interval. Thus, we set $\bar{\varepsilon} > 0$, which satisfying $|\dot{u}| \le \bar{\varepsilon}$. Because $e(t_i) = 0$, the least value of trigger intervals $t_{j+1} - t_j \ge \frac{\delta|u|+\hbar}{\bar{\varepsilon}}$. Thus, Zeno's behavior is avoided. Besides, the triggering condition relies on the control input computed from the quantized output signal, and the range of variation in the quantization interval is limited; thus, there is no Zeno phenomenon.

IV. Numerical Simulation

The efficacy of the proposed DETOQC scheme is illustrated via the finite difference method in MATLAB. Table I provides the system parameters. The time and space steps are 1.5×10^{-4} and 2.095×10^{-2}, respectively. The initial conditions of the FSLM are specified as $\omega(s,0) = 0$ m, $\dot{\omega}(s,0) = 0$ m/s, $\theta(0) = 0$ rad, and $\dot{\theta}(0) = 0$ rad/s. The parameters chosen for the DETOQC scheme are $h_1 = 0.3$, $h_2 = 0.01$, $\xi = 0.05$, $h_3 = 3.3$, and $\bar{\omega} = 0.13$. The reference signal, denoted by

TABLE I
STRUCTURE PARAMETER OF THE MODEL

Items	Value	Items	Value
I	0.0038 kgm^2	c	0.04NS/m
l	0.419 m	ρ	0.1 kg/m
T	0.1 N	EI	0.157 Nm^2

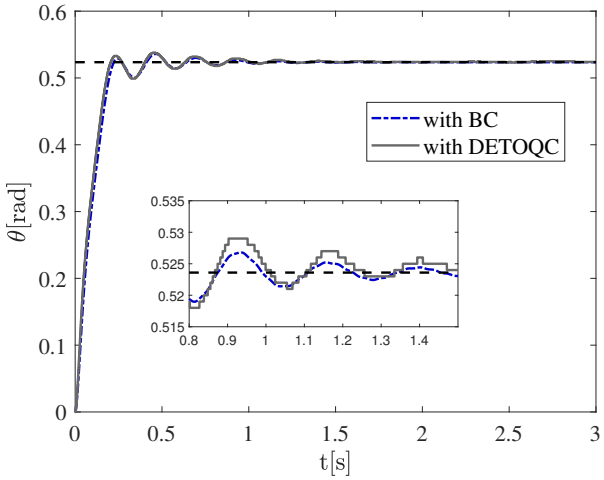

Fig. 4. The angular position of FSLM under different controllers.

θ_r, is assigned the value of $\frac{\pi}{6}$ rad. The adaptive parameters are elected as: $\hbar(0) = 0.01$, $\lambda = 0.3$, and $\delta = 0.2$. The quantization parameters are $d = 0.001$ and $\omega_{\min} = 10^{-3}$.

To demonstrate the effectiveness of the DETOQC scheme in saving communication resources, we first compare it to the boundary control (BC) scheme presented in [35] which was constructed using the same initial conditions. The simulation results are presented in Figs. 4-7. The BC method is based on continuous state variables and was designed without dynamic ETM. It is expressed as

$$u(t) = -k\gamma - k_1\omega_l - T\omega_l - \beta I\dot{\theta}(t) - k_\theta[\theta(t) - \theta_r] \quad (31)$$

where the BC parameters are defined as k = 0.28, k_1 = 0.01, and k_θ = 4.7. The angle position and the angular velocity is shown in Fig. 4. Fig. 5 displays the endpoint displacement of the flexible link. Fig. 6 illustrates the actuator control signals, and the event-triggered intervals of the control signal are given in Fig. 7.

As indicated in Fig. 4, θ can rapidly approach the given target angle θ_r within 0.5 seconds, and the steady-state tracking error finally stabilizes in a small bounded region within 1.5 seconds under the BC strategy and the DETOQC. Fig. 5 also shows that the deformation can attain convergence within a time interval of 2 seconds and remains confined to a small vicinity of zero under the BC strategy the DETOQC. The control inputs are displayed in Fig. 6, indicating that the input signals under the boundary control and dynamic event-triggered quantization control strategies are transmitted within the same period and under event-triggered intervals, respectively. Fig. 7 depicts the dynamic event-triggered intervals for the FSLM system. The total number of triggers is 181. To

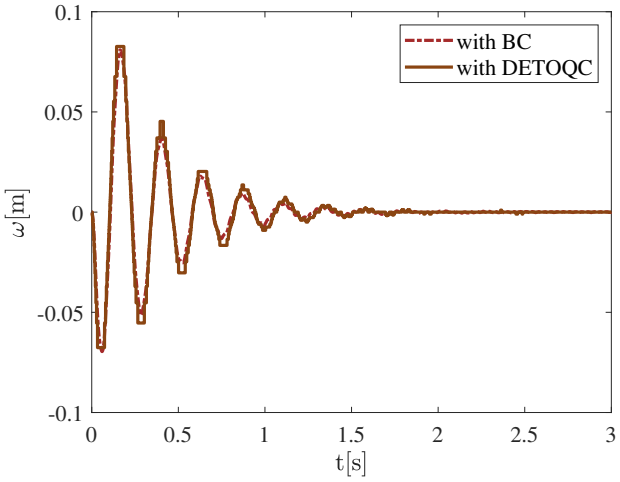

Fig. 5. The end-point offset of FSLM under different controllers.

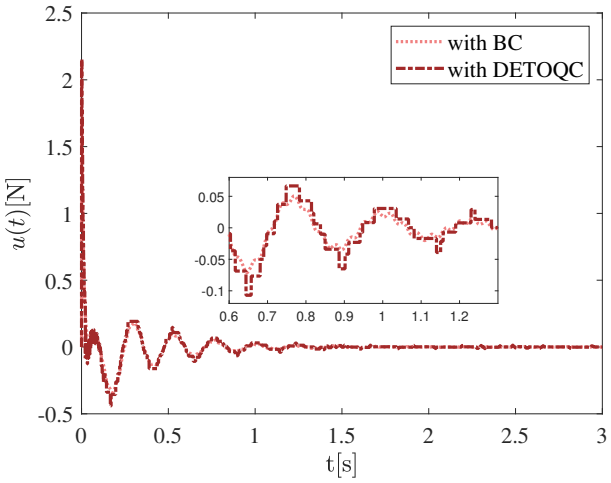

Fig. 6. The control signals of FSLM under controllers.

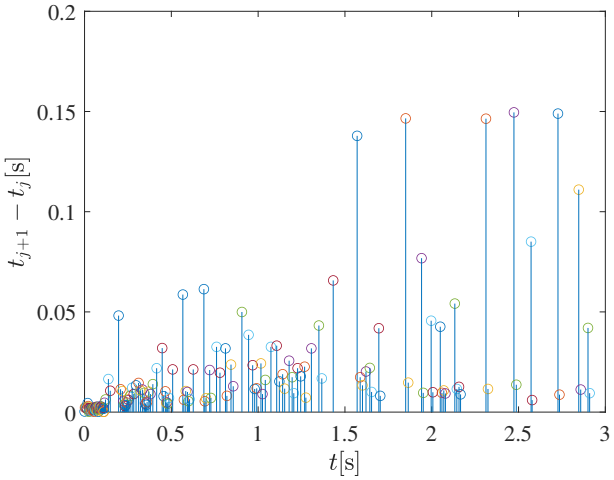

Fig. 7. Event-triggered intervals of the actuator.

TABLE II
QUANTITATIVE COMPARISON OF BC AND DETOQC SCHEMES

Performance Indicator	**Boundary Control (BC) [32]**	**DETOQC**	**Improvement Ratio**
Angular Tracking Time (to steady state, s)	1.5	1.5	— (Equivalent Performance)
Steady-State Angular Error (rad)	≤ 0.008	≤ 0.007	12.5%
Tip Vibration Convergence Time (s)	2.0	1.9	5.0%
Steady-State Tip Vibration (m)	≤ 0.012	≤ 0.009	25.0%
Total Control Signal Transmissions (in 3 s)	2860	181	93.7%
Average Trigger Interval (ms)	— (No Triggering Mechanism)	16.5	—

TABLE III
STRUCTURE PARAMETER OF THE MODEL IN EXPERIMENT

Items	Value
h_3	3
ξ	0.02
h_1	0.01

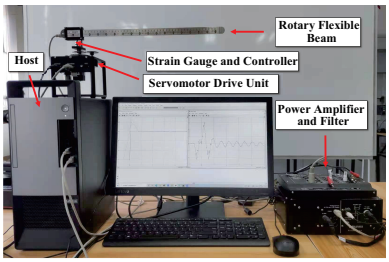

Fig. 8. Rotary flexible manipulator system.

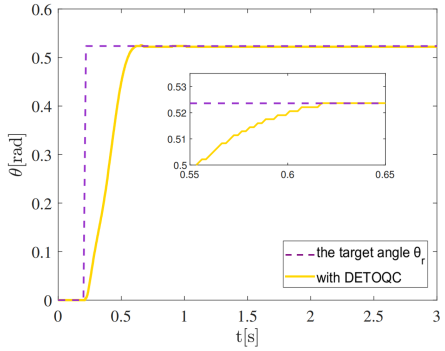

Fig. 9. Angular position of the FSLM.

further quantify the performance advantages of the proposed DETOQC scheme, Table III summarizes the key performance indicators of the BC scheme [32] and the DETOQC scheme.

From Figs. 2-5, we can conclude that this method can achieve performance similar to control strategies designed based on ideal continuous signals, and under adaptive dynamic event-triggered control, the transmission frequency of control signals is significantly reduced. This implies that only a small number of signals need to be transmitted, thereby reducing transmission costs.

By analysing the simulation results, significantly decrease the communication frequency and maintain system performance at reduced communication frequencies. In the aforementioned event-triggered strategy, when the magnitude of the control signal $u_r(t)$ increases, a longer update interval is obtained, resulting in relatively larger measurement errors. When the system state stabilizes within a small region near zero, the control signal correspondingly decreases to a smaller range, producing smaller thresholds and thereby allowing more accurate control of the system, resulting in improved system performance. It is noteworthy that due to its adaptive nature, the dynamic event-triggered strategy offers better adjustment capability, simplified parameter settings, and broader applicability to different systems.

V. EXPERIMENT

To demonstrate the actual applications of the DETOQC scheme, practical experiments are performed on the Quanser experimental platform depicted in Fig. 8. The experiment use the ode4 (Runge-Kutta) fixed-step solver, with the time step set to $T_s = 1$ms. After adjusting the system, the selected appropriate gain parameters are presented in the Table III (the remaining parameters are consistent with those used in the simulation). The experimental results are presented in Figs. 9-11. Fig. 9 presents the rotation angle, and the time delay for the target signal is set to 0.2 seconds. The manipulator can follow the desired trajectory within 0.5 seconds. The endpoint deformation is shown in Fig. 10, which can converge to a small neighborhood near zero within 1 second. The control input is shown in Fig. 11. Note that the output signals are quantified and the control signal is event-triggered. These experimental examples demonstrate that the dynamic event-triggered control strategy can ensure the angle tracking and deformation suppression performance of the flexible robotic arm while reducing the communication frequency.

VI. CONCLUSION

This study developed a dynamic event-triggered control strategy to address the communication bandwidth constraints, achieve superior angle-tracking performance, and suppress vibrations in the FSLM systems. The output signals were quantized, and an internal dynamic variable was employed to optimize the triggering mechanism. Moreover, the Lyapunov direct method was utilized to demonstrate the uniformly bounded stability of the closed-loop system. Simulations and experiments verified that the proposed method achieved a

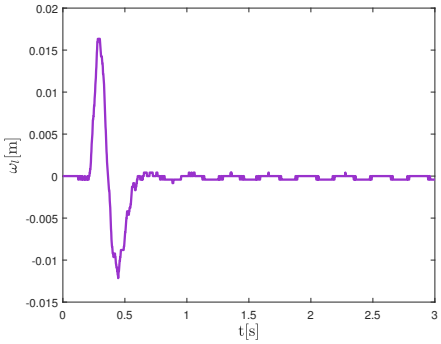

Fig. 10. The endpoint deformation of the FSLM.

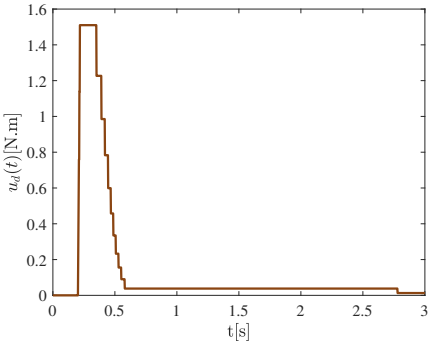

Fig. 11. Torque of the motor.

similar performance compared to the BC method, in which the signal is continuously transmitted. The former only needed less signal transmission.

APPENDIX A

Proof: Using Young's Inequality and Sobolev's inequality, we derive

$$\begin{aligned}|L_{k3}(t)| &\le \xi\rho\int_0^l |\dot{\varpi}\omega|ds + \xi\rho l\int_0^l |\dot{\varpi}[\theta(t)-\theta_r]|ds \\ &\le \frac{\xi\rho(1+l)}{2}\int_0^l \dot{\varpi}^2 ds + \frac{\xi\rho l^2}{2}\int_0^l \omega'^2 ds \\ &\quad + \frac{\xi\rho l^2}{2}[\theta-\theta_r]^2 \le \xi_1(L_{k1}(t)+L_{k2}(t)) \end{aligned} \tag{32}$$

where $\xi_1 = \xi\max(\rho(1+l), \frac{\rho l^2}{T}, \frac{\rho l^2}{h_3})$. Let ξ satisfy $0<\xi_1<1$; then we have

$$\begin{aligned}0 &\le \psi_1(L_{k1}(t)+L_{k2}(t)+L_{k3}(t)) \le L_k(t) \\ &\le \psi_2(L_{k1}(t)+L_{k2}(t)+L_{k3}(t)) \end{aligned} \tag{33}$$

where ψ_1=min1-ξ_1, and ψ_2=max1+ξ_1. □

APPENDIX B

Proof: Differentiating (17), we obtain

$$\dot{L}_k(t) = \dot{L}_{k1}(t) + \dot{L}_{k2}(t) + \dot{L}_{k3}(t) \tag{34}$$

First, applying the integration by parts and invoking Young's Inequality and Sobolev's inequality, $\dot{L}_{k1}$ can be expressed as

$$\begin{aligned}\dot{L}_{k1}(t) &= \rho\int_0^l \dot{\varpi}\ddot{\varpi}ds + EI\int_0^l \omega''\dot{\omega}''ds + T\int_0^l \omega'\dot{\omega}'ds \\ &= T\int_0^l s\dot{\theta}\omega''ds - \flat\int_0^l \dot{\varpi}^2 ds - EI\omega_0''\dot{\theta} - EIl\dot{\theta}(t)\omega_l''' \\ &\le -EI\omega_0''\dot{\theta}(t) - T\dot{\theta}(t)\omega_l - \flat\int_0^l \dot{\varpi}^2 ds \end{aligned} \tag{35}$$

Next, we take the derivative of $L_{k3}(t)$, and obtain

$$\begin{aligned}\dot{L}_{k3}(t) &= \xi\rho\int_0^l \ddot{\varpi}\varpi_d ds + \xi\rho\int_0^l \dot{\varpi}^2 ds \\ &= \xi\rho\int_0^l \ddot{\varpi}[\omega + z(\theta(t)-\theta_r)]ds + \xi\rho\int_0^l \dot{\varpi}^2 ds \\ &= -\xi EI\omega_l\omega_l''' - \xi EI\int_0^l \omega'^2 ds + T\xi\omega_l'\omega_l \\ &\quad - T\xi\int_0^l \omega'^2 ds - \xi EI[\theta(t)-\theta_r]\omega_0'' \\ &\quad - \xi\flat\int_0^l \varpi_d\dot{\varpi}ds - T\xi[\theta(t)-\theta_r]\omega_l \\ &\quad + \xi\rho\int_0^l \dot{\varpi}^2 ds \end{aligned} \tag{36}$$

Finally, substituting (2) and the adaptive law (9) into the derivative of the function $L_{k2}(t)$, we obtain

$$\begin{aligned}\dot{L}_{k2}(t) &= \gamma I(\ddot{\theta} + \xi\dot{\theta}) + h_3[\theta(t)-\theta_r]\dot{\theta} + \dot{\hbar} \\ &= \gamma I\xi\dot{\theta}(t) + \gamma T\omega_l + \gamma EI\omega_0'' + \gamma u_r(t) \\ &\quad + h_3[\theta(t)-\theta_r]\dot{\theta}(t)\dot{\hbar} - \lambda\hbar + |\gamma|(\delta|u| - |e|) \end{aligned} \tag{37}$$

Owing to the fact that $u_r(t) - u(t) \le |u_r(t) - u(t)|$, and considering properties (5) and (11), we have

$$\begin{aligned}\dot{L}_{k2}(t) &\le \gamma I\xi\dot{\theta}(t) + \gamma T\omega_l + \gamma EI\omega_0'' + \gamma(1+\lambda_1\delta)u(t) \\ &\quad + h_3[\theta(t)-\theta_r]\dot{\theta}(t) - \lambda\hbar \end{aligned} \tag{38}$$

where $\lambda_1 \in [-1, 1]$.
Using the DETOQ controllers (15)-(16), and combining (13)-(14), we obtain

$$\begin{aligned}\gamma(1+\lambda_1\delta)u(t) &\le -h_1\gamma^2 - \gamma(T+h_2)\omega_{lU}^Q - \gamma\xi I\dot{\theta} \\ &\quad - \gamma h_3(\theta-\theta_r) + \upsilon \\ &\le -h_1\gamma^2 - (T+h_2)\gamma\omega_l - \gamma\xi I\dot{\theta} + \upsilon \\ &\quad - h_3\gamma(\theta-\theta_r) - \gamma(T+h_2)\mu\omega_{l\min} \\ &\quad - \gamma\bar{\omega}\tanh(\frac{\gamma\bar{\omega}}{J}) \end{aligned} \tag{39}$$

subsequently, substituting (39) into $\dot{L}_{k2}(t)$ yields

$$\begin{aligned}\dot{L}_{k2}(t) &\le \gamma I\xi\dot{\theta}(t) + \gamma T\omega_l + \gamma EI\omega_0'' - h_1\gamma^2 - \gamma\xi I\dot{\theta} \\ &\quad - (T+h_2)\gamma\omega_l - \gamma(T+h_2)\mu\omega_{l\min} - \gamma\bar{\omega}\tanh(\frac{\gamma\bar{\omega}}{J}) \\ &\quad - h_3\gamma(\theta-\theta_r) - \lambda\hbar + h_3\dot{\theta}[\theta-\theta_r] + \upsilon \\ &\le -h_1\gamma^2 + \gamma EI\omega_0'' - \gamma h_2\omega_l - h_3[\theta(t)-\theta_r]^2 \\ &\quad - \lambda\hbar + \varepsilon \end{aligned} \tag{40}$$

where $\varepsilon = 0.2875J + \upsilon$. By combining (35)-(36) into (34), $\dot{L}_k(t)$ can be derived as

$$\begin{aligned}\dot{L}_j(t) \leq & -(\flat - \hbar\rho - \frac{\hbar\flat(1+l)}{2}) \int_0^l \dot{\varpi}^2 ds \\ & - (\xi h_3 - \frac{\xi\flat l^2}{2})[\theta(t) - \theta_r]^2 + \varepsilon - \lambda\hbar \\ & - (T\xi - \frac{\xi\flat l^2}{2} - \frac{(h_2+T)l}{2\varsigma_2}) \int_0^l \omega'^2 ds \\ & - (h_1 - \frac{(h_2+T)\varsigma_2}{2} - \frac{1}{\varsigma_1})\gamma^2 - \xi EI \int_0^l \omega''^2 ds \end{aligned} \tag{41}$$

where ς_1 and $\varsigma_2 > 0$.

Parameters ξ, h_1, h_2, h_3, ς_1, ς_2, ς_3, and ς_4 are chosen to satisfy the following inequalities

$$\jmath_1 = \flat - \xi\rho - \frac{\xi\flat(1+l)}{2} > 0 \tag{42}$$

$$\jmath_2 = T\xi - \frac{\xi\flat l^2}{2} - \frac{(h_2+T)l}{2\varsigma_2} > 0 \tag{43}$$

$$\jmath_3 = \xi h_3 - \frac{\xi\flat l^2}{2} > 0 \tag{44}$$

$$\jmath_4 = h_1 - \frac{(h_2+T)\varsigma_2}{2} - \frac{1}{\varsigma_1} > 0 \tag{45}$$

$$\psi_3 = \min(2\jmath_1/\rho, 2\jmath_2/T, 2\jmath_3/h_3, 2\jmath_4/I, 2\xi, \bar{\lambda}) \tag{46}$$

In the simulation section, we adjust the above parameters to meet the requirements of inequality constraints. Then, invoking (42)-(45), we obtain

$$\begin{aligned}\dot{L}_k(t) \leq & -\jmath_1 \int_0^l \dot{\varpi}^2 ds - \xi EI \int_0^l \omega'^2 ds - \jmath_3 \int_0^l \omega''^2 ds \\ & - \jmath_4[\theta(t) - \theta_r]^2 - \jmath_5\gamma^2 - \bar{\lambda}\hbar + \varepsilon \end{aligned} \tag{47}$$

Combining (33) and (36), we obtain

$$\dot{L}_k(t) \leq -\psi L_k(t) + \varepsilon \tag{48}$$

where $\psi = \frac{\psi_3}{\psi_2} \geq 0$. □

REFERENCES

[1] H. Ren, L. Cao, H. Ma, and H. Li, "Dynamic event-triggered-based fuzzy adaptive pinning control for multiagent systems with output saturation," *IEEE Transactions on Fuzzy Systems*, vol. 33, no. 4, pp. 1277–1286, 2025.

[2] D. Qin, J. Wu, A. Liu, W.-A. Zhang, and L. Yu, "Cooperation and coordination transportation for nonholonomic mobile manipulators: A distributed model predictive control approach," *IEEE Transactions on Systems, Man, and Cybernetics: Systems*, vol. 53, no. 2, pp. 848–860, 2022.

[3] D. Li, H.-G. Han, and J.-F. Qiao, "Composite boundary structure-based tracking control for nonlinear state-dependent constrained systems," *IEEE Transactions on Automatic Control*, vol. 69, no. 8, pp. 5686–5693, 2024.

[4] N. Jiang, S. Zhang, J. Xu, and D. Zhang, "Model-free control of flexible manipulator based on intrinsic design," *IEEE/ASME Transactions on Mechatronics*, vol. 26, no. 5, pp. 2641–2652, 2021.

[5] A. Alessandri, M. Baglietto, and G. Battistelli, "Receding-horizon estimation for discrete-time linear systems," *IEEE Transactions on Automatic Control*, vol. 48, no. 3, pp. 473–478, 2003.

[6] W. He, F. Kang, L. Kong, Y. Feng, G. Cheng, and C. Sun, "Vibration control of a constrained two-link flexible robotic manipulator with fixed-time convergence," *IEEE Transactions on Cybernetics*, vol. 52, no. 7, pp. 5973–5983, 2022.

[7] H. Gao, W. He, C. Zhou, and C. Sun, "Neural network control of a two-link flexible robotic manipulator using assumed mode method," *IEEE Transactions on Industrial Informatics*, vol. 15, no. 2, pp. 755–765, 2019.

[8] S. Zhang, R. Liu, K. Peng, and W. He, "Boundary output feedback control for a flexible two-link manipulator system with high-gain observers," *IEEE Transactions on Control Systems Technology*, vol. 29, no. 2, pp. 835–840, 2021.

[9] Y. Ren, Z. Zhao, C. Zhang, Q. Yang, and K.-S. Hong, "Adaptive neural-network boundary control for a flexible manipulator with input constraints and model uncertainties," *IEEE Transactions on Cybernetics*, vol. 51, no. 10, pp. 4796–4807, 2021.

[10] Y. Liu, W. Zhan, M. Xing, Y. Wu, R. Xu, and X. Wu, "Boundary control of a rotating and length-varying flexible robotic manipulator system," *IEEE Transactions on Systems, Man, and Cybernetics: Systems*, vol. 52, no. 1, pp. 377–386, 2022.

[11] S. Chen, Z. Zhao, D. Zhu, C. Zhang, and H.-X. Li, "Adaptive robust control for a spatial flexible timoshenko manipulator subject to input dead-zone," *IEEE Transactions on Systems, Man, and Cybernetics: Systems*, vol. 52, no. 3, pp. 1395–1404, 2022.

[12] Y. Ma, X. He, S. Zhang, Y. Sun, and Q. Fu, "Adaptive compensation for infinite number of actuator faults and time-varying delay of a flexible manipulator system," *IEEE Transactions on Industrial Electronics*, pp. 1–1, 2022.

[13] S. Zhang, Y. Wu, X. He, and Z. Liu, "Cooperative fault-tolerant control for a mobile dual flexible manipulator with output constraints," *IEEE Transactions on Automation Science and Engineering*, vol. 19, no. 4, pp. 2689–2698, 2022.

[14] G. Pin, G. Fenu, V. Casagrande, D. Zorzenon, and T. Parisini, "Robust stabilization of a class of nonlinear systems controlled over communication networks," *IEEE Transactions on Automatic Control*, vol. 66, no. 7, pp. 3036–3051, 2021.

[15] Y. Zhang, J.-F. Zhang, X.-K. Liu, and Z. Liu, "Quantized-output feedback model reference control of discrete-time linear systems," *Automatica*, vol. 137, p. 110027, 2022.

[16] L. Xing, C. Wen, Y. Zhu, H. Su, and Z. Liu, "Output feedback control for uncertain nonlinear systems with input quantization," *Automatica*, vol. 65, pp. 191–202, 2016.

[17] Y. Liu, X. Yao, and W. Zhao, "Distributed neural-based fault-tolerant control of multiple flexible manipulators with input saturations," *Automatica*, vol. 156, p. 111202, 2023.

[18] J. Wang, H. Yang, J. Liu, and S. Wang, "Quantization control for flexible manipulators with pde model," *Asian Journal of Control*, vol. 24, no. 6, pp. 3117–3132, 2022.

[19] J. Wang and J. Liu, "Event-triggered boundary quantization control for flexible manipulator based on partial differential equations dynamic model," *Transactions of the Institute of Measurement and Control*, vol. 43, no. 9, pp. 2111–2123, 2021.

[20] X. Zhao, S. Zhang, Z. Liu, J. Wang, and H. Gao, "Adaptive event-triggered boundary control for a flexible manipulator with input quantization," *IEEE/ASME Transactions on Mechatronics*, vol. 27, no. 5, pp. 3706–3716, 2022.

[21] S. M. Schlanbusch, J. Zhou, and R. Schlanbusch, "Adaptive attitude control of a rigid body with input and output quantization," *IEEE Transactions on Industrial Electronics*, vol. 69, no. 8, pp. 8296–8305, 2022.

[22] Z. Zhang, C. Wen, L. Xing, and Y. Song, "Adaptive output feedback control of nonlinear systems with mismatched uncertainties under input/output quantization," *IEEE Transactions on Automatic Control*, vol. 67, no. 9, pp. 4801–4808, 2022.

[23] J. Huang, W. Wang, C. Wen, and G. Li, "Adaptive event-triggered control of nonlinear systems with controller and parameter estimator triggering," *IEEE Transactions on Automatic Control*, vol. 65, no. 1, pp. 318–324, 2020.

[24] Y. Hu, H. Yan, H. Zhang, M. Wang, and C. Chen, "Adaptive neural network output-feedback control for uncertain nonlinear systems via event-triggered output," *IEEE Transactions on Systems, Man, and Cybernetics: Systems*, vol. 54, no. 10, pp. 5864 – 5875, 2024.

[25] H. Xie, G. Zong, D. Yang, Y. Guo, and X. Zhao, "Secure control for switched nonlinear systems with dos attacks: A switching event-triggered adaptive output-feedback control method," *IEEE Transactions on Systems, Man, and Cybernetics: Systems*, vol. 54, no. 5, pp. 3011 – 3021, 2024.

[26] Z. Zhang, C. Wen, L. Xing, and Y. Song, "Adaptive event-triggered control of uncertain nonlinear systems using intermittent output only," *IEEE Transactions on Automatic Control*, vol. 67, no. 8, pp. 4218–4225, 2022.

[27] L. Xing, C. Wen, Z. Liu, H. Su, and J. Cai, "Event-triggered adaptive control for a class of uncertain nonlinear systems," *IEEE Transactions on Automatic Control*, vol. 62, no. 4, pp. 2071–2076, 2017.

[28] X. Zhao, S. Zhang, Z. Liu, and Q. Li, "Vibration control for flexible manipulators with event-triggering mechanism and actuator failures," *IEEE Transactions on Cybernetics*, vol. 52, no. 8, pp. 7591–7601, 2022.

[29] J. Wang and J. Liu, "Event-triggered boundary quantization control for flexible manipulator based on partial differential equations dynamic model," *Transactions of the Institute of Measurement and Control*, vol. 43, no. 9, pp. 2111–2123, 2021.

[30] A. Girard, "Dynamic triggering mechanisms for event-triggered control," *IEEE Transactions on Automatic Control*, vol. 60, no. 7, pp. 1992–1997, 2014.

[31] X. Ge and Q.-L. Han, "Distributed formation control of networked multi-agent systems using a dynamic event-triggered communication mechanism," *IEEE Transactions on Industrial Electronics*, vol. 64, no. 10, pp. 8118–8127, 2017.

[32] J. Wang, H. Yang, J. Liu, and S. Wang, "Quantization control for flexible manipulators with pde model," *Asian Journal of Control*, vol. 24, no. 6, pp. 3117–3132, 2022.

[33] L. Li and J. Liu, "Event-triggered boundary control of a flexible manipulator with uncertain end load," *International Journal of Control*, pp. 1–12, 2021.

[34] W. He, X. He, M. Zou, and H. Li, "Pde model-based boundary control design for a flexible robotic manipulator with input backlash," *IEEE Transactions on Control Systems Technology*, vol. 27, no. 2, pp. 790–797, 2019.

[35] X. He, S. Zhang, Y. Ouyang, and Q. Fu, "Vibration control for a flexible single-link manipulator and its application," *IET Control Theory & Applications*, vol. 14, no. 7, pp. 930–938, 2020.